Separation of Light Gas Mixtures Using SAPO-34 Membranes

Joseph C. Poshusta, Vu A. Tuan, Eric A. Pape, Richard D. Noble, and John L. Falconer
Dept. of Chemical Engineering, University of Colorado, Boulder, CO 80309

Continuous SAPO-34 membranes were prepared on porous alumina tubular supports, and shown to be useful for light gas separations at low and high temperatures. Single-gas permeances of CO_2, N_2 and CH_4 decreased with increasing kinetic diameter. For the best membrane at 300 K, the He and H_2 permeances were less than that of CO_2, because He, H_2, and CO_2 were small compared to the SAPO-34 pore, and differences in the heat of adsorption determined the permeance order. The smaller component permeated the fastest in CO_2/CH_4, CO_2/N_2, N_2/CH_4, H_2/CH_4 and H_2/N_2 mixtures between 300 and 470 K. For H_2/CO_2 mixtures, which were separated by competitive adsorption at room temperature, the larger component permeated faster below 400 K. The CO_2/CH_4 selectivity at room temperature was 36 and decreased with temperature. The H_2/CH_4 mixture selectivity was 8 and constant with temperature up to 480 K. Calcination, slow temperature cycles, and exposure to water vapor had no permanent effect on membrane performance, but temperature changes of approximately 30 K/min decreased the membrane's effectiveness.

Introduction

Zeolite and other inorganic molecular sieve membranes have shown potential for separations based on molecular size and shape because of their small pore sizes, typically less than 1 nm, and their narrow pore-size distribution. The high thermal and chemical stability of these inorganic crystals make them ideal materials for use in high-temperature applications such as catalytic membrane reactors. Most of the progress with zeolite membranes has been with MFI zeolite prepared on porous disks (Geus et al., 1993; 1992; Jansen et al., 1994; Lovallo et al., 1998; Matsukata and Kikuchi, 1997; Vroon, 1995; Yan et al., 1995) and tubes (Bai et al., 1995; Coronas et al., 1997; Giroir-Fendler et al., 1996; Jia et al., 1994; Kusakabe et al., 1996; Oh et al., 1997). The MFI zeolite is a medium pore-size structure having nearly circular pores with diameters between 0.53 and 0.56 nm. Separation experiments through MFI membranes indicate that competitive adsorption separates light gas mixtures (Bakker et al., 1996, 1993; Jia, et al., 1994; Kapteijn et al., 1995; Lovallo et al., 1998; Poshusta et al., 1999; van den Broeke et al., 1999; Vroon, 1995). Light gas selectivities are typically small, however, owing to small differences in adsorption strengths and their small sizes relative to the MFI pore opening. Furthermore, competitive adsorption does not work well at high temperature where zeolite membranes are stable and have potential application.

Separation by differences in size has a greater potential to work at high temperature than competitive adsorption, but pores smaller than those in MFI zeolites are required. Therefore, some studies focused on the synthesis of small, 8-membered-pore structures such as zeolite A (0.41-nm pore diameter) (Aoki et al., 1998; Masuda et al., 1995) and SAPO-34 (Lixiong et al., 1997; Poshusta et al., 1998), a chabazite (about 0.4-nm pore diameter with $\sim$1.4 nm cages) analog. The SAPO-34 structure is a silicoaluminophosphate having the composition $(Si_xAl_yP_z)O_2$ where $x = 0.01-0.98$, $y = 0.01-0.60$, $z = 0.01-0.52$, and $x + z = y$ (Szostak, 1989). The crystal structure of SAPO-34 crystals has not been analyzed to determine the pore size, but adsorption experiments using n-C_4H_{10} (0.43 nm) and i-C_4H_{10} (0.50 nm) have shown that the SAPO-34 pore diameter is between 0.43 and 0.50 nm (Lok et al., 1984).

The smaller pore size of the zeolite A and SAPO-34 structures made the separation of smaller molecules by differences in size possible. Aoki et al. (1998) reported H_2/N_2 se-

Correspondence concerning this article should be addressed to J. L. Falconer.

lectivities through NaA zeolite membranes between 4.5 and 4.8, but the light gas permeances did not decrease with kinetic diameter, following the order $H_2 > O_2 > CH_4 > CO_2 = N_2 = C_3H_8$ instead. Lixiong et al. (1997) demonstrated that SAPO-34 membranes hold promise for separating light gas mixtures because ideal selectivities favored the smaller molecule, unlike MFI zeolite membranes. Previously, we also reported (Poshusta et al., 1998) that ideal selectivities correlated with molecule size and that SAPO-34 membranes were effective at separating CO_2/CH_4 mixtures with a selectivity of 30 at room temperature.

X-Ray diffraction (XRD) studies have shown that SAPO-34 crystals are stable up to 1,273 K, but further heating to 1,373 K breaks down the SAPO-34 structure (Watanabe, et al., 1993). The crystal structure, as measured by XRD, is affected by water adsorption, but calcination at 573 K in a dry environment recovers the SAPO-34 XRD pattern (Vomscheid et al., 1993; Watanabe et al., 1993). Vomscheid et al., (1993) showed that, when hydrated, Si−O−Al bonds open to form Si−OH and Al-OH bonds. Briend and coworkers (1995) found that prolonged exposure to water vapor permanently degrades SAPO-34 crystals, and the severity depends on the time and temperature of exposure to water vapor and the type of template used in the synthesis procedure. Above 373 K, SAPO-34 was highly stable in humid atmospheres, but below this temperature, the crystallinity and porosity were reduced. The crystallinity and porosity were completely recoverable after 2 days of hydration below 373 K by calcination, but long-term hydration (up to 2 years) had a permanent effect. They found that crystals made with tetraethylammonium hydroxide (TEAOH) template were more stable than those made with morpholine template, and retained 80% of their starting crystallinity and 70% of their porosity after a 2-year hydration. A measurable decrease in porosity of SAPO-34 crystals synthesized with the TEAOH template required at least a 10-day hydration.

The current study uses membranes that were prepared under slightly different conditions from our earlier study (Poshusta et al., 1998) so that their permeances are significantly higher. We demonstrate the ability of SAPO-34 membranes to separate light gas mixtures and describe the mechanisms governing these separations. Six membranes were prepared to investigate their morphology, separation ability, reproducibility, and stability. Single-gas and binary-gas mixture permeances were measured at various temperatures and pressures, and the membrane resistance to water vapor, temperature cycles, and calcination was investigated.

Experimental Methods

The SAPO-34 membranes were prepared by hydrothermal synthesis on the inside surface of asymmetric, porous α-alumina tubes (U.S. Filter) having 0.2-μm pores on the inside surface. To avoid bypass, the ends of the tubes were sealed with a glazing compound (GL 611A, Duncan), which was applied by dip coating about 1 cm of each end, and then heated at a rate of 1.2 K/min to 1193 K in air and held there for 30 min. The glazed supports were cleaned twice in an ultrasonic water bath at 313 K for 10 min, boiled in distilled water at 368 K for 1 h, and dried under vacuum at 373 K for 30 min.

The synthesis gel had the molar composition: $Al_2O_3 : P_2O_5 : 0.6\ SiO_2 : 1.07$ TEAOH $: 56\ H_2O$, and was prepared by stirring H_3PO_4, Al(i-$C_3H_7O)_3$, and H_2O at room temperature for 5 h. Then the template molecule, TEAOH, was added and the mixture stirred for 30 min before the silica sol (Ludox AS40) was added to the mixture. This solution was stirred for 2 h at room temperature to obtain a homogeneous solution, and the finished gel was stored in a covered glass beaker until used.

The membranes were synthesized using a procedure similar to that of Bai et al. (1995) for MFI zeolites, and was the same procedure previously used for SAPO-34 membranes (Poshusta et al., 1998). In the previous study (Poshusta et al., 1998), SAPO-34 was synthesized by filling the support tube with synthesis gel, sealing the tube in an autoclave, and immediately placing the autoclave in an oven for synthesis at 468 K for 20 h. In the current study, the support tube was filled with the synthesis gel, which soaked into the pores of the support for 2−24 h. The tube was refilled with gel, the tube ends were wrapped with Teflon tape, and the tube was placed in the autoclave for hydrothermal synthesis. In the current study, the synthesis temperature was lowered to 458 K and synthesis was carried out for 24 h. This change reduced the SAPO-34 crystallization rate. After synthesis, the membranes were washed and dried as described previously (Poshusta et al., 1998), and additional layers were applied until the membranes were impermeable to N_2 at 300 K. To remove the template molecules, impermeable membranes were then calcined at 753 K for 8 h with a 0.6-K/min heating rate. After calcination, the n-C_4H_{10} flux was measured for some membranes, and membranes were considered good if the n-C_4H_{10} permeance was below the minimum detectable limit [7×10^{-11} mol/(m^2·s·Pa)]. Before further permeation experiments, these membranes were calcined at 573 K for 10 h to remove adsorbed n-C_4H_{10}. The 10-h duration is probably longer than necessary, but it was convenient because the calcination program ran overnight and the exposure to room temperature air was minimized.

Single-gas and mixture permeation was measured on a system similar to that used by Funke et al. (1996), but modified for the study of light gases at higher pressures, as described elsewhere (Poshusta et al., 1998). The membranes were mounted in a stainless-steel module, and sealed at each end with silicone O-rings. The pressure on each side of the membrane could be independently controlled between 84 and 770 kPa, and the module temperature was controlled between 300 and 530 K with an electrically heated oven. Feed gases could be humidified by bubbling them through water, and the composition of water vapor was measured using a gas chromatograph. Fluxes were measured using a soap-film bubble flowmeter and a stopwatch. The estimated permeance measurement error was 2%, and the lowest measurable permeance was estimated to be 7×10^{-11} mol/(m^2·s·Pa).

All single-gas and mixture permeances were measured as a function of temperature and pressure without a sweep gas under a constant pressure drop of 138 kPa. Constant pressure-drop operation reveals more information about nonzeolite pore behavior than experiments where the pressure drop varies, because surface diffusion through zeolite pores and viscous and Knudsen flow through nonzeolite pores increase with increasing pressure drop (Poshusta et al., 1999). As pressure is increased at constant pressure drop, however, surface

diffusion (for Langmuir adsorption) through zeolite pores decreases, viscous flow increases, and Knudsen flow is constant. The pressure-drop method also eliminates back permeation of the sweep gas used in the Wicke-Kallenbach method. Indeed, van de Graaf et al. (1998) showed that a permeate sweep gas affects permeation because of competitive adsorption and counterdiffusion.

Before the single-gas permeances were measured, the feed and permeate sides of the membrane were evacuated and then swept with the gas to be studied while the membrane was heated to 473 K to desorb gases that may interfere with the measurement. Single-gas permeances were measured in dead-end mode (retentate stream blocked) for He, H_2, CO_2, N_2, and CH_4. The ideal selectivity is the ratio of the single-gas permeances. Binary mixtures of CO_2/CH_4, CO_2/N_2, N_2/CH_4, H_2/CH_4, H_2/CO_2, and H_2/N_2 were separated at various temperatures and pressures. Mass flow controllers were used to mix pure gases in equimolar ratios, and the compositions of the feed, retentate, and permeate streams were measured using a gas chromatograph equipped with a thermal conductivity detector. Selectivity is defined as the ratio of the permeances of each gas in the mixture (also called permselectivity). Although selectivity defined this way is inadequate when comparing at different pressures (Poshusta et al., 1999), the permselectivity is useful to compare with ideal selectivities.

The thermal stability and resistance to water vapor of SAPO-34 membranes were investigated by several approaches. High-temperature stability was measured by continuously measuring the H_2/CH_4 selectivity at 523 K for several days. Cycling the temperature between 300 and 473 K, while separating a CO_2/CH_4 mixture, provided a check of the SAPO-34 membrane stability with temperature cycles. The membranes' resistance to calcination was checked by comparing the CO_2/CH_4 selectivity before and after 12-h calcinations at 573 K. Likewise, the CO_2/CH_4 selectivity determined the effect of thermal shock after heating the membrane to 458 K and quickly cooling it to room temperature in about 5 min by flowing dry CO_2 over the membrane. The effect of humidity on membrane performance was measured by exposing membranes to humidified CO_2/CH_4 mixtures and then heating the membrane to 473 K with a dry CO_2/CH_4 feed to drive off adsorbed water. The CO_2/CH_4 selectivity was measured after the water exposure and drying to discern any membrane degradation due to water.

Results

Membrane preparation and morphology

The SAPO-34 membranes used in this study are listed in Table 1. Every membrane required four synthesis layers to be impermeable to N_2 at 300 K before template removal. After calcination, the permeance of n-C_4H_{10} was measured for membranes M1 and M2 as an initial indication of membrane quality. After the single-gas and mixture permeances of the light gases were measured, the n-C_4H_{10} permeance was measured through membranes M3 and M6. The n-C_4H_{10} permeance through membrane M3 was less than our minimum detectable permeance of 7×10^{-11} mol/(m^2·s·Pa). The n-C_4H_{10} permeance through a previous SAPO-34 membrane, M1* (Poshusta et al., 1998), was also below the minimum detection limit and had a CO_2/CH_4 selectivity of 30 at room temperature. The results in Table 1 show that the membranes with the highest n-C_4H_{10} permeances had the lowest CO_2/CH_4 selectivities. Membrane M1 had the lowest CO_2/CH_4 selectivity and was therefore broken for scanning electron microscopy (SEM) analysis. Membrane M2 was calcined to remove adsorbed n-C_4H_{10} before further permeation measurements. The n-C_4H_{10} permeance was not measured through membranes M4 and M5 to avoid a second calcination before further permeation experiments.

Table 1. Room-Temperature Membrane Permeation Properties

Memb.	Init. n-C_4H_{10} Permeance $\times10^9$ [mol/(m^2·s·Pa)]	CO_2/CH_4 Mixture Selectivity	CO_2/CH_4 Mixture Flux $\times10^3$ [mol/(m^2·s)]
M1	70	10	1.7
M2	1.2	18	1.2
M3	< 0.07*	36	3.4
M4	Not measured	16	19
M5	Not measured	14	2.3
M6	4.8	26	4.8
M1**	< 0.07	30	0.48

*The n-C_4H_{10} permeance was measured after single gas and mixture experiments.
**Membrane M1* was reported in a previous study as membrane M1 (Poshusta et al., 1998).

The X-ray diffraction pattern of the uncalcined powder formed in the synthesis gel after hydrothermal synthesis is shown in Figure 1. A calcined sample would have an open porous structure to water vapor, which is known to change the SAPO-34 structure and XRD pattern (Briend, et al., 1995). The main peaks of the XRD pattern in Figure 1 match those of uncalcined SAPO-34 crystals reported by Xu et al. (1990), and they are also consistent with the *d*-spacings of SAPO-34 reported by Lok et al. (1984) and Meier and Olson (1992). The high intensity of the XRD lines and the low background intensity indicate a high degree of crystallinity.

SEM images of membrane M1 are shown in Figures 2 and 3. The SEM photograph of the surface of the membrane (Figure 2) shows a continuous layer of intergrown cubic crystals 3–4μm in diameter. Smaller crystals (less than 1μm) were

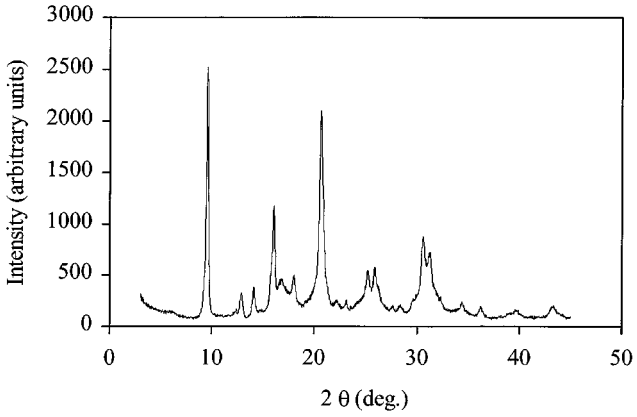

Figure 1. XRD spectrum of uncalcined SAPO-34 powder.

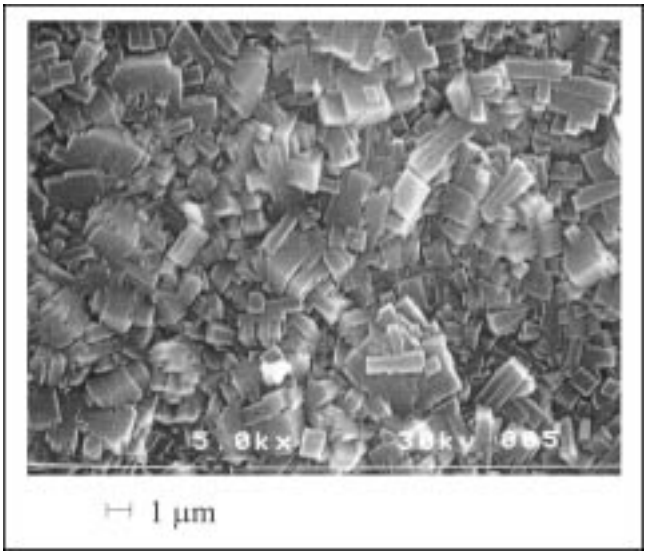

Figure 2. SEM image of the surface of SAPO-34 membrane M1.

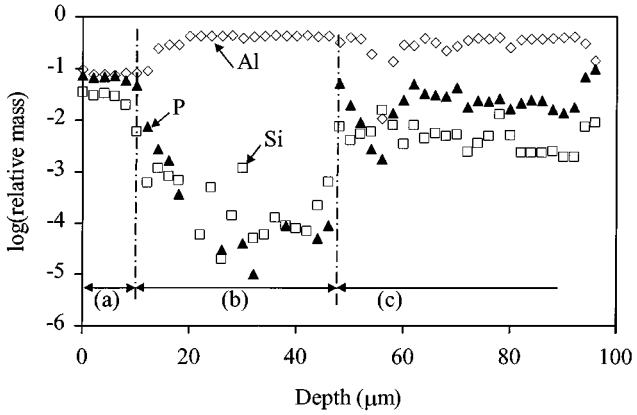

Figure 4. EMPA analysis of the cross section of SAPO-34 membrane M1 showing the concentrations of Si, Al, and P as a function of depth from the membrane surface.

Region (a) is the SAPO-34 layer, region (b) is the 40 μm thick, 0.2-μm pore-size support layer, and region (c) is the course alumina support layer.

also on the surface and many were in the boundaries between the larger crystals. The SEM image of the membrane cross section (Figure 3) shows that the SAPO-34 layer was 5–10μm thick. The SEM measurements could not distinguish if SAPO-34 crystals are in the pores of the support.

Electron microprobe analysis of the cross section showed that the thickness of the SAPO-34 layer was about 10 μm [Figure 4, region (a)]. Silicon and phosphorous penetrated the support, indicating that SAPO-34 crystals or amorphous material may have formed inside the porous support structure. Region (b) in Figure 4 corresponds to the 0.2-μm pore-size surface layer of the asymmetric support, and region (c) is within the coarse layer of the support. The Si and P concentrations decreased within the 0.2-μm pore support structure due to the lower porosity of this layer. The Si and P concentrations were higher in the coarse support layer, because of its larger void volume. The surface crystals had an average atomic ratio of 0.18 Si : 0.47 Al : 0.36 P, as determined by electron microprobe analysis of the SAPO-34 layer [Figure 4, region (a)]. Elemental analysis of the surface layer by energy dispersive spectroscopy (EDS) gave an atomic ratio or 0.11 Si : 0.48 Al : 0.41 P. These ratios are consistent with those required for the SAPO-34 structure (Szostak, 1989).

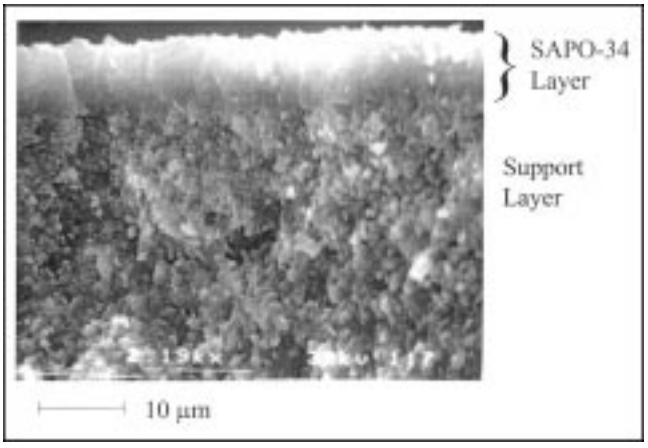

Figure 3. SEM image of the cross section of SAPO-34 membrane M1.

Single-gas permeation

Single-gas permeances of He, H_2, CO_2, N_2, CH_4, and *n*-C_4H_{10}, measured at room temperature and 270 kPa feed pressure, are shown as a function of kinetic diameter in Figure 5. Membrane M1* [from a previous study (Poshusta et al., 1998)] is also included, and the permeances through this membrane were less than those through membranes M2 and M3. These permeances were measured after a series of other

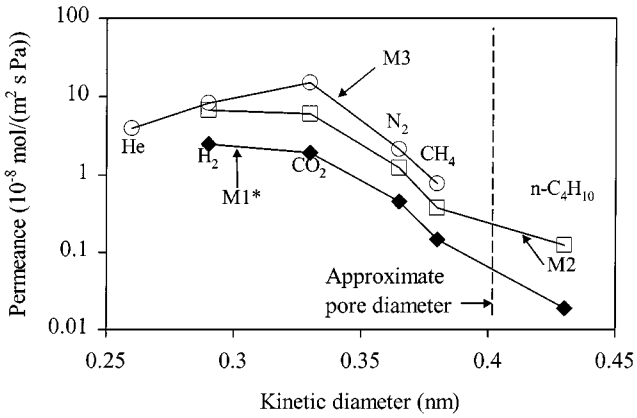

Figure 5. Room-temperature permeances at a feed pressure of 270 kPa and pressure drop of 138 kPa through membranes M2, M3, and M1* (Poshusta, et al., 1998) as a function of the gas kinetic diameter.

The *n*-C_4H_{10} permeance through membrane M3 was less than 7×10^{-11} mol/(m^2·s·Pa).

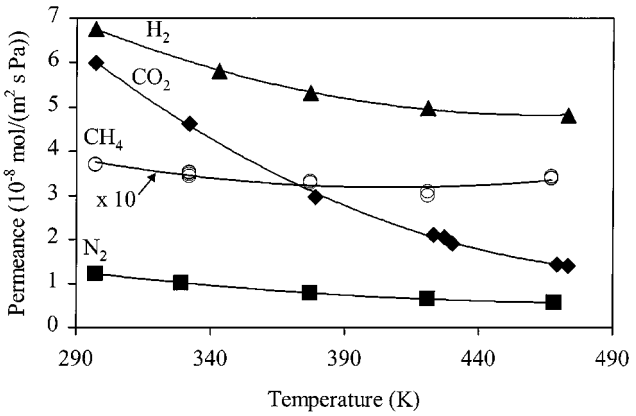

Figure 6. Single gas permeances through SAPO-34 membrane M2 as a function of temperature with a feed pressure of 270 kPa and a pressure drop of 138 kPa.

Note that the CH_4 permeance was multiplied by 10 to make it easier to see.

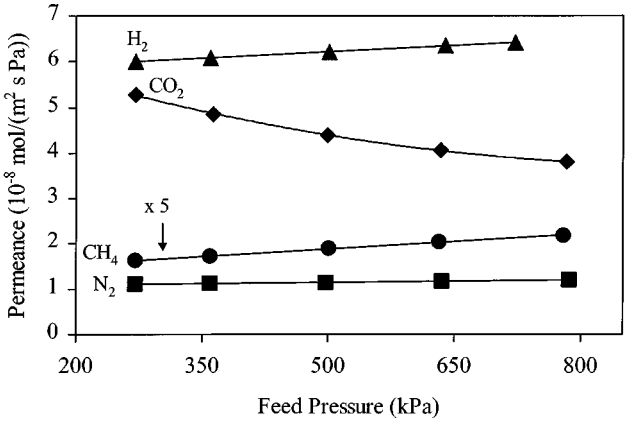

Figure 8. Single gas permeances through SAPO-34 membrane M2 as a function of pressure at room temperature with a 138-kPa pressure drop.

Note that the CH_4 permeance was multiplied by 5 to make it easier to see.

experiments and two 10-h calcinations at 573 K. Note that the permeance for n-C_4H_{10} in membrane M1* is higher than the minimum detectable limit reported in Table 1, because the properties of this membrane changed. Also note that the permeance of n-C_4H_{10} through membrane M3 measured after single-gas and mixture permeance experiments was less than the minimum detectable limit of 7×10^{-11} mol/(m^2·s·Pa). For membranes M2 and M1*, the single-gas permeances decreased with kinetic diameter. Through membrane M3, however, the permeances of molecules larger than CO_2 (0.33 nm) decrease with kinetic diameter, but the He (0.26 nm) and H_2 (0.29 nm) permeances are less than that of CO_2.

The effect of temperature on the single-gas permeances of He, H_2, CO_2, N_2, and CH_4 is shown in Figures 6 and 7 for membranes M2 and M3, respectively. Although the order of the permeances of He, H_2, and CO_2 are different for membranes M2 and M3, their temperature dependencies are similar. The temperature dependence of the CO_2 permeance through these membranes is similar to that observed previously (Poshusta et al., 1998). We (Poshusta et al., 1998) found previously that the single-gas permeances of H_2 and N_2 displayed minima, and CH_4 increased with temperature, unlike the results in Figures 6 and 7. Note that membranes M2 and M3 were synthesized at 458 K for 24 h, but membrane M1* was synthesized at 468 K for 20 h.

In our previous study (Poshusta et al., 1998), the permeances of H_2, CO_2, N_2, and CH_4 decreased with increasing feed pressure at constant pressure drop. Except for CO_2 the permeances of the light gases increased slightly with pressure through membrane M2, however, as shown in Figure 8. The permeances of He, H_2, N_2, and CH_4 are unaffected by pressure in membrane M3 (Figure 9). Differences in the pressure dependence of different membranes has been attributed to the presence of nonzeolite pores allowing Knudsen and viscous flow (Poshusta et al., 1999).

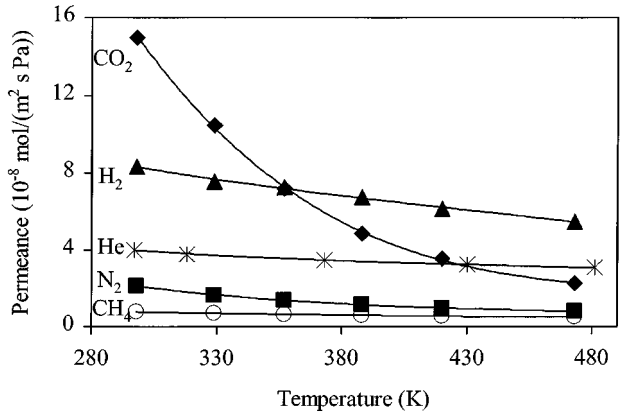

Figure 7. Single gas permeances through SAPO-34 membrane M3 as a function of temperature with a feed pressure of 270 kPa and a pressure drop of 138 kPa.

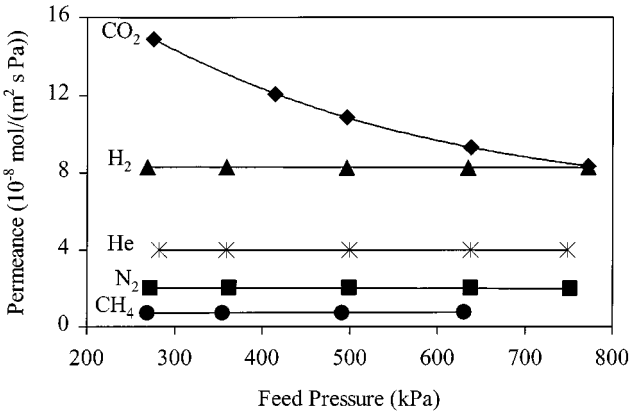

Figure 9. Single-gas permeances through SAPO-34 membrane M3 as a function of pressure at room temperature with a 138-kPa pressure drop.

Table 2. Ideal Selectivities at 270 kPa with 138 kPa Pressure Drop

	Ideal Selectivity					
	300 K			473 K		
Mixture	M3	M2	M1*	M3	M2	M1*
CO_2/CH_4	20	16	19	4.5	4.2	2.3
CO_2/N_2	7.1	4.9	5.7	2.8	2.5	2.0
N_2/CH_4	2.8	3.3	3.4	1.6	1.7	1.2
H_2/CH_4	11	18	25	11	14	7.4
H_2/N_2	4.0	5.5	7.5	6.8	8.5	6.4
H_2/CO_2	0.56	1.1	1.3	2.4	3.5	3.2

Membrane M1 was reported in a previous study as membrane M1 (Poshusta, et al., 1998).

The ideal selectivities of the light gases at a feed pressure of 270 kPa and a pressure drop of 138 kPa through membranes M2 and M3 are compared with those of membrane M1* at 300 and 473 K in Table 2. At 300 and 473 K, the ideal selectivities of CO_2/CH_4, CO_2/N_2, and N_2/CH_4 do not vary much between the three membranes. The H_2/CH_4 ideal selectivity decreases with temperature more for membrane M1* than the other two membranes. For H_2/N_2, the ideal selectivity increases for membranes M2 and M3, but decreases for membrane M1*. Again, note that membrane M1* was synthesized at 468 K for 20 h, but membranes M2 and M3 were synthesized at 458 K for 24 h.

Mixture permeation

Equimolar binary mixtures of H_2, CO_2, N_2, and CH_4 were separated with membranes M3 and M4, and a CO_2/CH_4 mixture was separated with membranes M1, M2, and M5. Table 1 compares the room-temperature CO_2/CH_4 separation selectivity and total mixture flux for each membrane. Compared with membrane M1*, the CO_2/CH_4 selectivities are about the same or smaller, but the fluxes are significantly higher, especially for membrane M4. Table 3 shows that the mixture selectivities of membranes M3, M4, and M5 are higher than the Knudsen selectivity for most of the mixtures (though not for H_2/N_2 and H_2/CO_2). Thus, light gases are not separated by Knudsen diffusion in these SAPO-34 membranes.

Membrane M3 has the highest selectivities, and the temperature dependence of each light gas binary mixture was measured. Figure 10 shows the fluxes of CO_2 and CH_4 and the selectivity through membrane M3 between 300 and 470 K. Both ideal and mixture selectivities are greater than one

Table 3 Mixture Selectivities

	Mixture Selectivity					
	M3		M4	M5		
Mixture	300 K	473 K	300 K	300 K	Knudsen Selectivity	Separation Regime
H_2/CH_4	8.4	7.9	7.1	4.1	2.8	1
H_2/N_2	3.3	5.1	2.7	—	3.7	1
N_2/CH_4	2.9	1.7	2.9	—	0.76	1
CO_2/N_2	16	3.2	6.4	—	0.80	3
CO_2/CH_4	36	5.2	16	14	0.60	3 (enhanced)
H_2/CO_2	0.25	2.1	0.42	—	4.7	3 (competing)

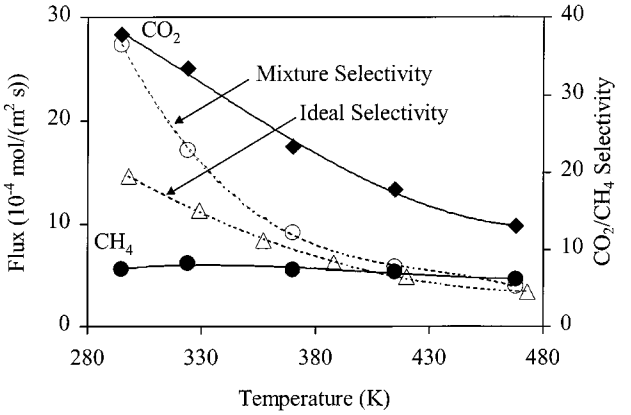

Figure 10. Fluxes and selectivity of a 50/50 CO_2/CH_4 mixture as a function of temperature for membrane M3 with a feed pressure of 270 kPa and a pressure drop of 138 kPa.

over the temperature ranges shown, and they follow roughly the same trend; the selectivity decreases as temperature increases. Note that at 300 K, the flux ratio is 5.1 and the mixture selectivity (permeance ratio) is about 36. This difference in ratios is due to the small partial pressure difference of CO_2 across the membrane in the mixture that gives a high CO_2 permeance and consequently a high CO_2/CH_4 selectivity. The separation of CO_2 and N_2 is shown in Figure 11, where the temperature dependencies of the ideal and mixture selectivities are similar to those of the CO_2/CH_4 mixture. The fluxes of CO_2 and N_2 also behave similarly to the CO_2 and CH_4 fluxes in Figure 10. The selectivity of the N_2/CH_4 mixture also decreases with temperature, as shown in Figure 12, and the ideal and mixture selectivities are nearly identical.

The H_2/CH_4 selectivity (Figure 13) is relatively constant at about 8 between room temperature and 486 K, whereas the H_2/N_2 selectivity (Figure 14) increases with temperature. For the H_2/CH_4 and H_2/N_2 mixtures, the smaller molecule H_2

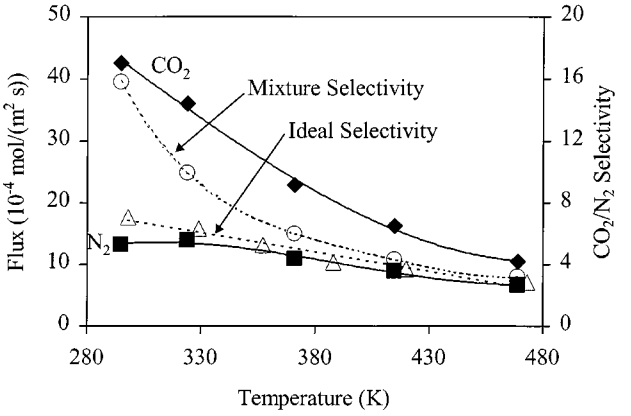

Figure 11. Fluxes and selectivity of a 50/50 CO_2/N_2 mixture as a function of temperature for membrane M3 with a feed pressure of 270 kPa and a pressure drop of 138 kPa.

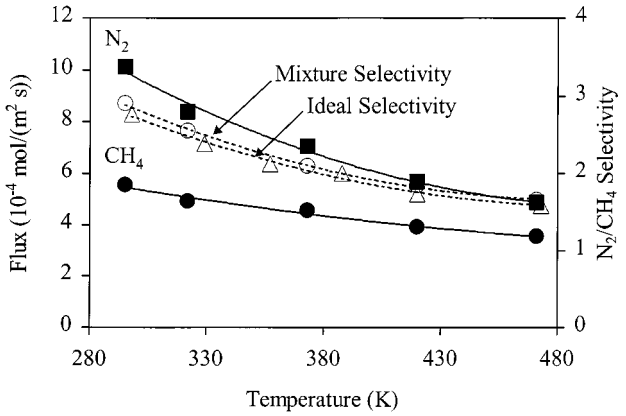

Figure 12. Fluxes and selectivity of a 50/50 N_2/CH_4 mixture as a function of temperature for membrane M3 with a feed pressure of 270 kPa and a pressure drop of 138 kPa.

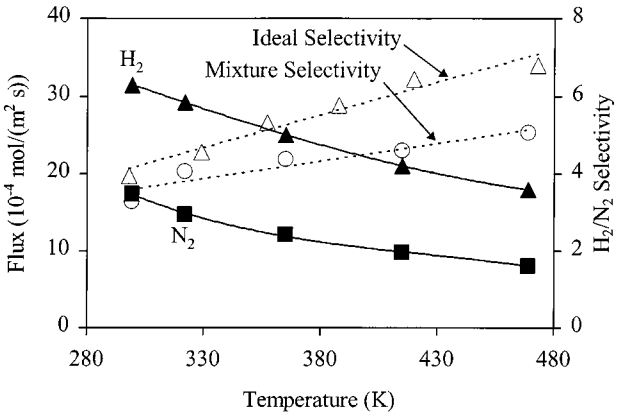

Figure 14. Fluxes and selectivity of a 50/50 H_2/N_2 mixture as a function of temperature for membrane M3 with a feed pressure of 270 kPa and a pressure drop of 138 kPa.

permeates faster than the larger molecule. In contrast, the H_2/CO_2 selectivity at room temperature is 0.56; the larger molecule (CO_2) permeates faster. As temperature increases, the H_2/CO_2 selectivity increases, and at about 370 K the H_2/CO_2 selectivity is greater than one, as shown in Figure 15. The ideal and mixture selectivities of H_2/CO_2 have similar temperature trends.

For each mixture, the fluxes of the individual components change with temperature like their corresponding single-gas permeances (Figure 7), except for H_2 in the H_2/CO_2 mixture. In CH_4-containing mixtures, the CH_4 flux is weakly dependent on temperature, and changes in the selectivity with temperature are primarily due to changes in the flux of the smaller molecule (such as H_2, CO_2, or N_2).

Membrane stability

For membrane M1*, the CO_2/CH_4 selectivity decreased irreversibly during the 8 months that permeation measurements were run. Since temperature cycles, calcination, or exposure to water vapor could be responsible, the effects of these treatments were studied for membranes M3, M5, and M6.

Membrane M3 was exposed to a humidified CO_2/CH_4 mixture a total of 6 h in 1-h increments. The total flux of the humidified mixture decreased from the dry value of 3.4×10^{-3} mol/(m^2·s) to about 4.1×10^{-4} mol/(m^2·s). After each 1-h exposure, the system was flushed with the dry CO_2/CH_4 mixture, and the membrane was heated to 473 K overnight to remove adsorbed water. After the membrane cooled to room temperature, the selectivity and mixture flux returned to the membrane's original values of 36 and 3.4×10^{-3} mol/(m^2·s). A seventh exposure to water vapor for 20 h decreased the mixture flux to 3.0×10^{-4} mol/(m^2·s), and the CO_2/CH_4 selectivity decreased to 0.74. The system was then flushed with the dry CO_2/CH_4 mixture at 473 K for 47 h and at 300 K for 72 h. The room temperature selectivity and flux returned to the original dry-membrane values. Similarly, humidification of the CO_2/CH_4 feed mixture decreased the selectivity of

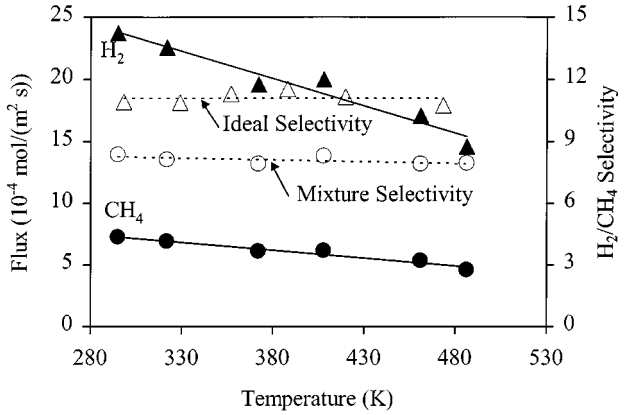

Figure 13. Fluxes and selectivity of a 50/50 H_2/CH_4 mixture as a function of temperature for membrane M3 with a feed pressure of 270 kPa and a pressure drop of 138 kPa.

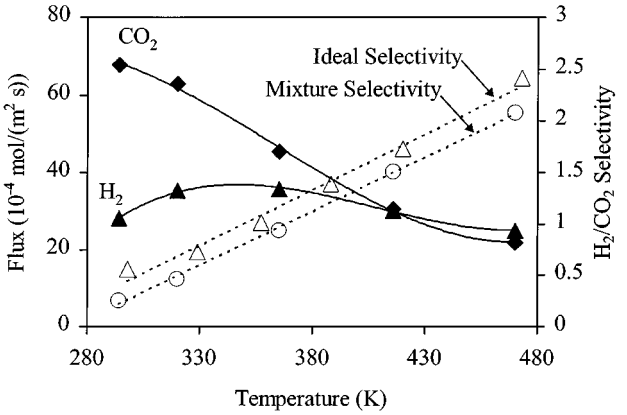

Figure 15. Fluxes and selectivity of a 50/50 H_2/CO_2 mixture as a function of temperature for membrane M3 with a feed pressure of 270 kPa and a pressure drop of 138 kPa.

membrane M5 to one, and the dry CO_2/CH_4 selectivity recovered to 15 after sweeping the membrane with dry CO_2 for 4 days at room temperature.

The thermal stability of the SAPO-34 membranes was also investigated. The H_2/CH_4 separation selectivity of membrane M5 was measured for 120 h at 473 K, and the selectivity (5.6) and mixture flux did not change. Membranes were calcined in an electrically heated furnace with a 0.6 K/min heating rate and a 1.2 K/min cooling rate. The CO_2/CH_4 selectivity and mixture flux of membrane M5 were unaffected after each of four 12-h calcinations at 573 K. The single-gas permeation of CO_2 as a function of pressure was also unchanged after each calcination. For membrane M6, the original CO_2/CH_4 selectivity at room temperature was 26 with a mixture flux of 4.8×10^{-3} mol/(m^2·s). The membrane was calcined twice, once for 12 h at 573 K and a second time for 10 h at 573 K. After the calcinations, the CO_2/CH_4 selectivity was 25 and 28, respectively, and each time the flux was 4.4×10^{-3} mol/(m^2·s).

For membrane M5, the room temperature CO_2/CH_4 separation selectivity was about 14 and was unaffected by four temperature cycles between room temperature and 473 K. Throughout the course of experiments on membrane M3, the CO_2/CH_4 selectivity did not decrease, and the mixture flux remained about the same after 14 temperature cycles between 300 and 473 K. Each of the temperature cycles was conducted within the gas permeation module at heating and cooling rates of about 3 K/min. Faster temperature changes degraded membrane M6, however. This membrane was heated outside the module to 458 K in an electrically heated oven and then quickly cooled while flowing dry CO_2 at 300 K over the membrane. The membrane cooled at a rate of about 30 K/min. The CO_2/CH_4 selectivity decreased to 19 (from an original value of 26) and the total mixture flux increased to 5.9×10^{-4} mol/(m^2·s) (from an original value of 4.8×10^{-4} mol/(m^2·s). Before the effects of thermal shock on the membranes was known, some membranes were removed from the calcination oven at about 370 to 420 K and immediately placed in the module under flowing CO_2 or N_2 to reduce the amount of water adsorption from the laboratory atmosphere. This may be the cause of the degradation of membrane M1*.

Discussion

Membrane stability

On the basis of CO_2/CH_4 selectivity, membranes M3 and M1* represent the best SAPO-34 membranes, but the CO_2/CH_4 selectivity of membrane M1* decreased to 10 during the course of permeation experiments. Temperature cycles with heating and cooling rates less than 1.2 K/min and exposure to water vapor were shown to have no permanent effect on the performance of membranes M3 and M5. Calcination also had no effect on the performance of membranes M5 and M6. Temperature changes of about 30 K/min degraded membrane performance by formation of non-SAPO-34 pores, because the membrane flux increased and the CO_2/CH_4 selectivity decreased. Nonzeolite pores that allow viscous and Knudsen flow have been shown to decrease the selectivity of zeolite membranes (Poshusta et al., 1999). Thermal shock probably introduced non-SAPO-34 pores into membrane M1*. Thus, if rapid temperature changes are avoided, the SAPO-34 membranes appear to be quite stable to conditions they might encounter during usage.

Single-gas permeation

The single-gas permeation dependence on the kinetic diameter in Figure 5 agrees with the SAPO-34 membrane results reported previously, except for H_2, which has a lower permeance than CO_2 for membrane M3 (Lixiong et al., 1997; Poshusta et al., 1998). The single-gas permeation of He, not measured in the other SAPO-34 studies, was less than that of H_2, although the kinetic diameter of He is smaller than that of H_2. Helium also permeates slower than H_2 in MFI membranes (Bakker et al., 1996). Because He and H_2 are small, their permeation is not hindered much by size restriction in SAPO-34 and MFI pores, and the size difference between He and H_2 has a small effect on determining the order of their permeances. Therefore, differences in adsorption are more important in determining permeance. This is analogous to single-gas permeances through MFI zeolite membranes, where CH_4 permeates faster than CO_2 at room temperature even though CO_2 is smaller (Bakker et al., 1997; Poshusta et al., 1999).

Single-gas permeation through zeolite and molecular sieve membranes is described as activated diffusion of an adsorbed phase using the surface diffusion model. This model describes the diffusion behavior well at low temperatures where the flux is proportional to an activated diffusivity and the gradient in chemical potential of the adsorbed gas (Vroon, 1995). The diffusivity and its activation energy depend on the type of gas and zeolite, and in general, diffusivity decreases with increasing kinetic diameter (Kärger and Ruthven, 1992). For light gases, the heat of adsorption does not correlate with molecular size, and it strongly affects the chemical potential gradient. Thus, CO_2 can permeate faster than He and H_2 even though CO_2 is the larger molecule.

The temperature variation of flux predicted by the surface diffusion model depends on the temperature dependencies of diffusivity and concentration within the zeolite pores. Diffusion through zeolite pores is activated, and therefore the diffusivity increases with temperature. The effect of temperature on changes in adsorbed concentration is more complicated, however. At a given pressure drop, the concentration gradient predicted by the Langmuir isotherm is small at low temperature where the coverage is nearly saturated. As the temperature increases, the coverage decreases, but the concentration gradient increases, because the slope of the isotherm is greater at lower coverages (for a given pressure) than when the surface is saturated. At high temperature, however, the adsorption approaches the Henry's regime, where increasing temperature decreases the slope of the isotherm. Therefore, the concentration gradient has a maximum with temperature, and because the chemical potential gradient is closely related to the concentration gradient, the gradient of chemical potential also has a maximum with temperature. In the surface diffusion model, the combination of the chemical potential gradient and the diffusivity can only describe permeances that increase, decrease, or exhibit a maximum with temperature. Some gases have minima in permeance for MFI zeolites, however (Coronas et al., 1997; Vroon, 1995). Likewise, the single-gas permeation of CH_4 ex-

hibits a minimum for membrane M2. Bakker et al. (1997) proposed that the minimum is due to a transition from surface diffusion to activated diffusion of a gaslike phase called gas translation diffusion.

Although this model can fit the temperature behavior of the single-gas permeances in the SAPO-34 membranes, it cannot explain why the permeance trends for some gases are different between membranes of the same molecular sieve. Permeation through nonzeolite pores may be responsible for these differences, and the presence of nonzeolitic pores was previously used to explain differences between membranes.(Coronas et al., 1997; Lin et al., 1998; Poshusta et al., 1999; van de Graaf, et al., 1999). These nonzeolite pores were viewed as intercrystalline pores, and permeation measurements made during calcination suggest non-zeolite pores open before the template is removed from the pores of the molecular sieve crystals (Lin et al., 1998; van de Graaf et al., 1999). Since membranes M1–M6 were made by the same procedure and they were impermeable to N_2 before calcination, the differences in their performance (Table 1) are probably due to the opening of nonzeolite pores during calcination. Different defect concentrations may be the result of impurities in the synthesis gel, differences in the starting support, or some small differences in preparation procedure.

Van de Graaf et al. (1999) characterized nonzeolite pores by measuring the temperature and pressure behavior of He and Ne single-gas permeances through a silicalite-1 membrane. The measurements indicated flow in both the Knudsen and viscous flow regimes. Poshusta et al. (1999) also demonstrated Knudsen and viscous flow behavior through MFI membranes by modeling the pressure dependence of CO_2 permeation and showed that membranes with more non-zeolite pores had lower CO_2/CH_4 selectivities. Membranes that exhibited viscous flow were not selective. Although viscous and Knudsen flow behaviors suggest pores larger than 1 nm, high mixture selectivities are observed through these membranes. Coronas et al. (1997), Lin et al. (1998), and Gump et al. (1999) suggested that most nonzeolite pores in high-quality membranes are near in size to the zeolite pores and selective, thus maintaining high selectivities while allowing for differences between membranes due to the varying concentrations of nonzeolite pores.

Flow associated with non-SAPO-34 pores can be identified by examining the effects of temperature and pressure on single-gas permeation. Quantifying the amount of nonzeolite pores by analyzing permeance vs. temperature data is difficult, because modeling surface diffusion requires heats of adsorption and activation energies for diffusion. This information is not available for SAPO-34, and the surface-diffusion model does not predict high-temperature behavior well. Poshusta et al. (1999), however, showed that nonzeolite pores can be characterized with fewer parameters by analyzing the flux vs. pressure at constant pressure drop. As pressure increases on both sides of the membrane, the surface-diffusion contribution through molecular sieve pores decreases, the viscous flow contribution increases linearly, and flow by Knudsen flow is constant.

A numerical application of this analysis to the data collected on membranes M2, M3, and M1* requires the Langmuir adsorption parameter, K, at room temperature, but adsorption studies of light gases on SAPO-34 are not published. We can qualitatively apply this analysis, however. The permeances of H_2, N_2, and CH_4 through membrane M2 increase with feed pressure at constant pressure drop, and viscous flow through nonzeolite pores must be present according to the model by Poshusta et al. (1999). An increase in the number of non-SAPO-34 pores lowers the selectivity, since the CO_2/CH_4 Knudsen selectivity is 0.6 and viscous flow is not selective. Indeed, membranes M3 and M1* (before it degraded) did not exhibit viscous flow behavior, because the light gas permeances did not increase with pressure at constant pressure drop, as shown in Figure 9 and the previous paper (Poshusta et al., 1998), and these membranes have higher CO_2/CH_4 selectivities than membrane M2.

The increase in non-SAPO-34 pores with membrane degradation also correlates with changes in the mixture selectivity; the original CO_2/CH_4 selectivity at room temperature for membrane M1* of 30 was reduced after degradation to 10, and the mixture flux increased by a factor of 10. Although the SAPO-34 molecular sieve structure and adsorption properties are stable up to 1273 K (Watanabe et al., 1993), thermal shock after calcination of the membrane is probably responsible for an increase in non-SAPO-34 pores and the degradation of the membrane.

Mixture permeation

The ideal selectivity was shown to be a poor indicator of the selectivity for light gas mixtures through MFI zeolite membranes, because for some mixtures the faster permeating component in the mixture was the slower permeating single gas (Bakker et al., 1996, 1993; Jia et al., 1994; Kapteijn et al., 1995; Poshusta et al., 1999; Vroon, 1995). The difference between ideal and mixture selectivities was attributed to separation by competitive adsorption, where the interactions of adsorbed gases cannot be accounted for by single-gas experiments. For SAPO-34 membranes, however, the ideal selectivity predicted the faster permeating component in the mixture for CO_2/CH_4, which lead to the conclusion that differences in diffusivity were important in the separation (Poshusta, et al., 1998). As previously seen for a CO_2/CH_4 mixture through SAPO-34 membranes (Poshusta et al., 1998), the mixture and ideal selectivities also correlate for the other light gas mixtures, but the CO_2/N_2 and CO_2/CH_4 mixture selectivities deviated the most from their ideal selectivities at low temperature. The differences between the Knudsen and the measured selectivities for the light gas mixtures shown in Table 3 indicate that separation was not by Knudsen diffusion through non-SAPO-34 pores.

The light gas separation results of the SAPO-34 membranes agrees with the model proposed by Keizer et al. (1998). This model, which was used to explain separation phenomena of light gas and hydrocarbon mixtures through MFI zeolite, states that both molecular sizes relative to the zeolite pore and the relative adsorption strengths determine the faster permeating species in a binary mixture. This gives rise to three separation regimes where both components are able to diffuse through the molecular sieve pores:

1. Differences in diffusivity: Both molecules have similar adsorption strengths, but one is larger and its diffusion is restricted due to pore walls. The membrane is selective for the smaller molecule.

2. Competitive adsorption: Both molecules have similar kinetic diameters, but one adsorbs more strongly. The membrane is selective for the strongly adsorbing molecule.

3. Combined differences in diffusivity and competitive adsorption: The molecules have significantly different diameters and adsorption strengths. The effects of each mechanism may combine to enhance separation or compete to reduce the selectivity. Regime 1 may be limited by single-file diffusion if molecules cannot pass one another inside the molecular sieve. This restricts the permeation of the component with the higher diffusivity, because it is blocked by the slower-moving component. Zeolites and molecular sieves that have interconnected pores and large cages may not be limited by single-file diffusion, because smaller molecules can pass one another within the cages or by diffusing around the cages through other pores. The SAPO-34 cage is $\sim$1.4 nm in diameter, which is more than the sum of the diameters of N_2 and CH_4, the largest pair of light gas molecules, and each cage has six pores. Thus, the light gas mixtures are not limited by single-file diffusion through SAPO-34 membranes, and light gases can be separated by differences in diffusivity.

Separation by competitive adsorption, regime 2, relies on the differences between the adsorption strengths of each molecule in the mixture. In this regime, the different molecules are competing for the same adsorption sites within the molecular sieve. The more strongly adsorbing molecule will be able to block the adsorption of the more weakly adsorbing one, and thus the membrane will be more selective for the strongly adsorbing molecule. At higher temperatures, the amount of adsorption decreases along with a molecule's ability to block adsorption sites. Therefore, the selectivity induced by competitive adsorption decreases with temperature.

Adsorption strengths are not available for light gases on SAPO-34, but we can infer the order of the adsorption strengths based on comparison with other zeolites. The heats of adsorption of light gases on NaA, CaA, NaX, NaY, CaY, H-chabazite, Na-mordenite, and H-mordenite increase in the order H_2, CH_4, N_2, and CO_2, except for a few cases where CH_4 has a higher heat of adsorption than N_2 (Breck 1974). This order is consistent with the electrostatic properties of each molecule. Carbon dioxide adsorbs the strongest because it has the strongest electrostatic quadrupole moment of the four gases, which contributes significantly to its attraction to polar surfaces, like those found in zeolites containing cations.

Table 3 shows which mechanism predominantly separates the light gas mixtures in this study. The H_2/CH_4 mixture is separated by regime 1, because neither molecule adsorbs strongly, and the CH_4 kinetic diameter (0.38 nm) is similar to the SAPO-34 pore diameter ($\sim$0.4 nm), but H_2 (0.29 nm) is much smaller, so H_2 diffuses faster. The H_2/N_2 mixture is also separated primarily by regime 1, but because N_2 is smaller than CH_4, the H_2/N_2 selectivities are smaller than the H_2/CH_4 selectivities. Nitrogen is slightly smaller than CH_4, so N_2 preferentially permeates in the N_2/CH_4 mixture, but the selectivity is low because of the small difference in size.

Because CO_2 adsorbs more strongly than the other gases, CO_2 preferentially permeates in CO_2/CH_4, CO_2/N_2, and H_2/CO_2 mixtures at low temperature. For the CO_2/CH_4 and CO_2/N_2 mixtures, CO_2 is also the smaller component and thus still permeates faster at high temperature. Also, the ideal and mixture selectivities are almost identical above 380 K for the CO_2/CH_4 and CO_2/N_2 mixtures (Figures 10 and 11). Thus, the CO_2/CH_4 mixture is separated by regime 3, where competitive adsorption (at low temperature) and differences in diffusivity combine to enhance selectivity. For the H_2/CO_2 mixture, however, separation is by regime 3, where competitive adsorption and differences in diffusivity compete, because CO_2 is the larger and more strongly adsorbing component. The H_2/CO_2 selectivity inversion is the transition between separation governed by competitive adsorption at low temperature and one governed by differences in diffusivity at high temperature.

Conclusions

Microporous SAPO-34 membranes were synthesized as 5–10 μm layers on the inside surface of porous α-alumina tubes. The membranes in this study had permeances 2.5–40 times higher than previous SAPO-34 membranes (Poshusta et al., 1998), but had similar CO_2/CH_4 selectivities. Freshly synthesized membranes have a low concentration of non-SAPO-34 pores, but their numbers increase with thermal shock, but do not increase with slow temperature cycles between 300 and 473 K, calcination at 573 K, and exposure to water vapor. Permeation of light gases through SAPO-34 membranes is a strong function of molecular size, but competitive adsorption is important in mixtures containing CO_2. The separation of CO_2/CH_4, CO_2/N_2, N_2/CH_4, H_2/CH_4, H_2/CO_2, and H_2/N_2 mixtures follow differences in diffusivities, but H_2/CO_2 separations are governed more by competitive adsorption below about 323 K. Competitive adsorption and differences in diffusivity combined to yield a CO_2/CH_4 selectivity of 36, but because competitive adsorption decreases with temperature, the CO_2/CH_4 selectivity was decreased at high temperature. The mixtures separated by differences in diffusivity had high selectivities at high temperature.

Acknowledgments

We gratefully acknowledge financial support by the DOE-PETC Contract DE-FG2698-FT40123. One of the authors (J.C.P.) acknowledges support by a Department of Education Graduate Assistantship in Areas of National Need, and another of the authors (E.A.P.) acknowledges support by the NSF Research Experience for Undergraduates Site Grant EEC-9531361. We also thank Sumesh Arora and Paul Schields of the Mississippi Chemical Corporation for performing the EDS analysis.

Literature Cited

Aoki, K., K. Kusakabe, and S. Morooka, "Gas Permeation Properties of A-type Zeolite Membrane Formed on Porous Substrate by Hydrothermal Synthesis," *J. Memb. Sci.*, **141**, 197 (1998).

Bai, C., M.-D. Jia, J. L. Falconer, and R. D. Noble, "Preparation and Separation Properties of Silicalite Composite Membranes," *J. Memb. Sci.*, **105**, 79 (1995).

Bakker, W. J. W., L. J. P. van den Broeke, F. Kapteijn, and J. A. Moulijn, "Temperature Dependence of One-Component Permeation through a Silicalite-1 Membrane," *AIChE J.*, **43**, 2203 (1997).

Bakker, W. J. W., F. Kapteijn, J. Poppe, and J. A. Moulijn, "Permeation Characteristics of a Metal-Supported Silicalite-1 Zeolite Membrane," *J. Memb. Sci.*, **117**, 57 (1996).

Bakker, W. J. W., G. Zheng, F. Kapteijn, M. Makkee, and J. A. Moulijn, "Single and Multi-Component Transport through Metal-

Supported MFI Zeolite Membranes,'' *Precis. Process Technol.*, 425 (1993).
Breck, D. W. *Zeolite Molecular Sieves*, Wiley, New York (1974).
Briend, M., R. Vomscheid, M. J. Peltre, P. P. Man, and D. Barthomeuf, ''Influence of the Choice of the Template on the Short- and Long-Term Stability of SAPO-34 Zeolite,'' *J. Phys. Chem.*, **99**, 8270 (1995).
Coronas, J., J. L. Falconer, and R. D. Noble, ''Characterization and Permeation Properties of ZSM-5 Tubular Membranes,''*AIChE J.*, **43**, 1797 (1997).
Funke, H. H., M. G. Kovalchick, J. L. Falconer, and R. D. Noble, ''Separation of Hydrocarbon Isomer Vapors with Silicalite Zeolite Membranes,'' *Ind. Eng. Chem. Res.*, **35**, 1575 (1996).
Geus, E. R., H. van Bekkum, W. J. W. Bakker, and J. A. Moulijn, ''High-Temperature Stainless Steel Supported Zeolite (MFI) Membranes: Preparation, Module Construction, and Permeation Experiments,'' *Microporous Mater.*, **1**, 131 (1993).
Geus, E. R., M. J. den Exter, and H. van Bekkum, ''Synthesis and Characterization of Zeolite (MFI) Membranes on Porous Ceramic Supports,'' *J. Chem. Soc., Faraday Trans.*, **88** 3101 (1992).
Giroir-Fendler, A., J. Peureux, H. Mozzanega, and J. A. Dalmon, ''Characterization of a Zeolite Membrane for Catalytic Membrane Reactor Application,'' *Stud. Surf. Sci. Catal.*, **101**, 127 (1996).
Gump, C. J., R. D. Noble, and J. L. Falconer, ''Separation of Hexane Isomers through Non-Zeolite pores in ZSM-5 Zeolite Membranes,'' *Ind. Eng. Chem. Res.*, **38**, 2775 (1999).
Jansen, J. C., D. Kashchiev, and A. Erdem-Senatalar, ''Preparation of Coatings of Molecular Sieve Crystals for Catalysis and Separation,'' *Adv. Zeolite Sci. Appl.*, **85**, 215 (1994).
Jia, M.-D., B. Chen, R. D. Noble, and J. L. Falconer, ''Ceramic-Zeolite Composite Membranes and Their Application for Separation of Vapor/Gas Mixtures,'' *J. Memb. Sci.*, **90**, 1 (1994).
Kapteijn, F., W. J. W. Bakker, J. van de Graaf, G. Zheng, J. Poppe, and J. A. Moulijn, ''Permeation and Separation Behavior of a Silicalite-1 Membrane,'' Catal. Today, **25**, 213, (1995).
Kärger, J., and D. M. Ruthven. *Diffusion in Zeolites*, Wiley, New York (1992).
Keizer, K., A. J. Burggraaf, Z. A. E. P. Vroon, and H. Verweij, ''Two Component Permeation through Thin Zeolite MFI Membranes,'' *J. Memb. Sci.*, **147**, 159 (1998).
Kusakabe, K., S. Yoneshige, A. Murata, and S. Morooka, ''Morphology and Gas Permeance of ZSM-5-Type Zeolite Membrane Formed on a Porous α-Alumina Support Tube,'' *J. Memb. Sci.*, **116**, 39 (1996).
Lin, X., J. L. Falconer, and R. D. Noble, ''Parallel Pathways for Transport in ZSM-5 Zeolite Membranes,'' *Chem. Mater.*, **10**, 3716 (1998).
Lixiong, Z., M. D. Jia, and M. Enze, ''Synthesis of SAPO-34/Ceramic Composite Membranes,'' *Stud. Surf. Sci. Catal.*, **105**, 2211 (1997).
Lok, B. M., C. A. Messina, R. L. Patton, R. T. Gajek, T. R. Cannan, and E. M. Flanigen, Crystalline Silicoalumino Phosphates, U.S. Patent No. 4,440,871 (1984).
Lovallo, M. C., A. Gouzinis, and M. Tsapatsis, ''Synthesis and Characterization of Oriented MFI Membranes and Films Prepared by Secondary Growth,'' *AIChE J.*, **44**, 1903 (1998).
Masuda, T., H. Hara, M. Kouno, H. Kinoshita, and K. Hashimoto, ''Preparation of an A-Type Zeolite Film on the Surface of an Alumina Ceramic Filter,'' *Microporous Mater.*, **3**, 565 (1995).
Matsukata, M., and E. Kikuchi, ''Zeolitic Membranes: Synthesis, Properties, and Prospects,'' *Bull. Chem. Soc. Jpn.*, **70**, 2341 (1997).
Meier, W. M., and D. H. Olson, *Atlas of Zeolite Structure Types*, 3rd ed., Butterworth-Heinemann, London (1992).
Oh, H.-S., M.-H. Kim, and H.-K. Rhee, ''Synthesis of ZSM-5 Zeolite Membrane on the Inner Surface of a Ceramic Tube,'' *Stud. Surf. Sci. Catal.*, **105**, 2217 (1997).
Poshusta, J. C., R. D. Noble, and J. L. Falconer, ''Temperature and Pressure Effects on CO_2 and CH_4 Permeation through MFI Zeolite Membranes,'' *J. Memb. Sci.*, **160**, 115 (1999).
Poshusta, J. C., V. A. Tuan, J. L. Falconer, and R. D. Noble, ''Synthesis and Permeation Properties of SAPO-34 Tubular Membranes,'' *Ind. Eng. Chem. Res.*, **37**, 3924 (1998).
Szostak, R. *Molecular Sieves— Principles of Synthesis and Identification*, Van Nostrand Reinhold, New York (1989).
Van de Graaf, J. M., F. Kapteijn, and J. A. Moulijn, ''Methodological and Operational Aspects of Permeation Measurements on Silicalite-1 Membranes,'' *J. Membr. Sci.*, **144**, 87 (1998).
Van de Graaf, J. M., F. Kapteijn, and J. A. Moulijn, ''Permeation of Weakly Adsorbing Components Through a Silicalite-1 Membrane,'' *Chem. Eng. Sci.*, **54**, 1081 (1999).
Van den Broeke, L. J. P., F. Kapteijn, and J. A. Moulijn, ''Transport and Separation Properties of a Silicalite-1 Membrane II. Variable Separation Factor,'' *Chem. Eng. Sci.*, **54**, 259 (1999).
Vomscheid, R., M. Briend, M. J. Peltre, P. Massiani, P. P. Man, and D. Barthomeuf, ''Reversible Modification of the Si Environment in Template-Free SAPO-34 Structure upon Hydration-Dehydration Cycles Below ca. 400 K,'' *J. Chem. Soc., Chem. Commun.*, **544** (1993).
Vroon, Z. A. E. P., ''Synthesis and Transport Studies of Thin Ceramic Supported Zeolite (MFI) Membranes,'' PhD. *Diss. Univ. of Twente*, Twente, The Netherlands (1995).
Watanabe, Y., A. Koiwai, H. Takeuchi, and S.-a. Hyodo, ''Multinuclear NMR Studies on the Thermal Stability of SAPO-34,'' *J. Catal.*, **143**, 430 (1993).
Xu, Y., P. J. Maddox, and J. W. Couves, ''The Synthesis of SAPO-34 and CoSAPO-34 from a Triethylamine-Hydrofluoric Acid-Water System,'' *J. Chem. Soc., Faraday Trans.*, **86**, 425 (1990).
Yan, Y., M. E. Davis, and G. R. Gavalas, ''Preparation of Zeolite ZSM-5 Membranes by In-Situ Crystallization on Porous α-Al_2O_3,'' *Ind. Eng. Chem. Res.*, **34**, 1652 (1995).

Manuscript received Apr. 9, 1999, and revision received Nov. 23, 1999.